Theory of radiation line-driven stellar winds

Jon Sundqvist, May 2024

1 Generic and simple supersonic radiation-driven wind outflow

The (non-viscous) hydrodynamical conservation equations of mass, momentum and energy can be written as

$$\frac{\partial \rho}{\partial t} \; + \; \nabla \cdot (\rho \mathbf{v}) \; = \; \mathbf{0} \tag{1}$$

$$\frac{\partial \rho \mathbf{v}}{\partial t} \; + \; \nabla \cdot (\mathbf{v} \rho \mathbf{v} + \mathrm{p_g} \mathbf{I}) = \; \mathbf{f} \tag{2}$$

$$\frac{\partial e}{\partial t} \; + \; \nabla \cdot (e \mathbf{v} + \mathrm{p_g} \mathbf{v}) \; = \; \dot{\mathrm{q}} \; + \; \mathbf{v} \cdot \mathbf{f} \tag{3}$$

which use total (kin.+int.) energy density $e \; = \; \frac{1}{2} \rho v^2 \; + \; \frac{p_g}{(\gamma - 1)} = \frac{1}{2} \rho v^2 + e_i$ for kinetic energy and internal energy with an adiabatic index γ.

The momentum source $\mathbf{f}$ can be, e.g.: external gravity $\mathbf{f} = \rho \mathbf{g} = -\rho \frac{GM_*}{r^2}$ (for a constant source mass M_*), the force due to magnetic fields or stellar rotation, or – *the key topic of this chapter* – a radiation force $\mathbf{f} = \rho \mathbf{g}_{\mathrm{rad}}$, where ρ is the mass density (g/cm^3 in cgs-units) and $\mathbf{g}_{\mathrm{rad}}$ the *radiative acceleration* (cm/s^2 in cgs).

Similarly, the energy sink/source terms $\dot{q}$ (appear next to work done by forces $\mathbf{v} \cdot \mathbf{f}$) can also contain radiation terms (radiative cooling and heating) as discussed previously.

Here we will use these equations for an isothermal ($T = Const.$, i.e. full energy equation will be dropped), spherically symmetric (only $\partial / \partial r \neq 0$ spatially), steady-state ($\partial / \partial t = 0$) stellar wind with gravity $g = GM/r^2$ and radiative acceleration g_{rad} as source terms. Then

$$\dot{M} = 4 \pi r^2 \rho v = Const. \tag{4}$$

$$v \frac{dv}{dr} \left(1 - \frac{a^2}{v^2} \right) = g_{\mathrm{rad}} - g + \frac{2a^2}{r} \tag{5}$$

and the energy equation can be replaced by the ideal gas law $p_g = a^2 \rho = \rho k_b T / (\mu m_H)$ for isothermal *gas* sound speed a, and where the mass-conservation equation has been used to eliminate ρ in the equation of motion.

1.1 An "anti-gravity" r^{-2} force

Since $g_{\rm rad} \sim F \sim 1/r^2$, it is useful to first consider a force on the simple form $\sim 1/r^2$, so that $\Gamma = g_{\rm rad}/g = Constant$. Consider now a massive star with $T \approx 40\,000$ K, $R_* \approx 20 R_\odot$, and $M \approx 20 M_\odot$. Then it is easy to show that the "Parker" term $2a^2/r$ at the stellar surface is only a small fraction of the local gravitational acceleration.

Exercise: For such a wind driven by $\Gamma = Const. > 1$, focus on the supersonic part $v \gg a$, neglect the "Parker term", and show that the equation of motion can be solved analytically from R_* assuming a vanishing $v(R_*)$, yielding $v(r) = v_\infty(1-R_*/r)^\beta$ with $\beta = 1/2$ and $v_\infty = v_{\rm esc}(R_*)\sqrt{\Gamma - 1}$.

1.2 General expressions of radiation force in stellar wind

As discussed in previous lectures, the radiative acceleration vector is

$$\mathbf{g}_{rad} = \frac{1}{\rho c} \int \oint \mathbf{n} \alpha_\nu I_\nu d\Omega d\nu \tag{6}$$

Note that this gives a 3D radiation force in general, and that we also now kept the possibility of an angle-dependent extinction α_ν (due to the Doppler shift when velocity-effects are non-negligible) with cgs-units $1/cm$.

1.2.1 Electron (Thomson) Scattering

As a simple example, consider first the extinction from continuum Thomson scattering (electron scattering, see Ch. 5 in Sundqivst's lecture-notes on "radiative processes"). Then $\alpha_\nu = \alpha_e$ is both frequency-independent and isotropic (the latter true at least in a fore-aft sense), so that

$$\mathbf{g}_e = \frac{\kappa_e \mathbf{F}}{c} \tag{7}$$

for an *opacity* (mass-absorption coefficient) $\kappa_e = \alpha_e/\rho$.

Exercise: [Repetition from "radiative processes"!] For a fully ionized plasma dominated by hydrogen and helium, with a helium number abundance $Y_{\rm He} = n_{He}/n_H = 0.1$ (representative of the Sun), show that $\kappa_e = 0.34\,{\rm cm}^2/{\rm g}$. For such a 'Thomson atmosphere', κ is indeed constant, as was implicitly assumed in the exercise above ($\Gamma = Const.$).

1.2.2 Dust scattering / absorption

Will be covered by Leen in next lecture... Now, we move on to

2 Spectral line force

In contrast to the electrons scattering case above, consider now instead a spectral line with extinction

$$\alpha_\nu^l = \alpha_L \phi(\nu - \nu_0) = \sigma_{cl} f_{lu} n \phi_\nu \tag{8}$$

where $\phi(\nu-\nu_0) = \phi_\nu$ is the line-profile function peaked at line-centre frequency ν_0, which is normalized such that $\int \phi_\nu d\nu = 1$, n the number density of the lower level in the considered transition, σ_{cl} the classical frequency-integrated line cross-section, and f_{lu} the quantum mechanical oscillator-strength correction for the line. Note that we have neglected the influence of stimulated emission in the above expression; this is quite ok e.g. for ultra-violet resonance lines, of key importance in hot star winds, but would become questionable if considering, e.g., molecular line-transitions in the infra-red. Again, you can read more about these line opacity quantities in Sundqvist's lecture-notes on "radiative processes", and also in Rutten's lecture-notes for the first part of this course.

Neglecting the impact of any additional continuum extinction, this gives for the radiation line-force

$$\mathbf{g}_{line} = \frac{\alpha_L}{\rho c} \int \oint \mathbf{n} \phi_\nu I_\nu d\Omega d\nu \tag{9}$$

2.1 Optically thin spectral line force

Assume now a spherically symmetric situation where the intensity I_ν streams from a central continuum source with constant values in the positive direction $\mu \geq 0$ and zero intensity for incoming directions $\mu \leq 0$ (think, e.g., of the surface of a star; radiation only flows outwards, escaping the star). If we then further assume that

i) this I_ν does not vary much over the extent of the line-profile (a good assumption since continuum radiation varies much more slowly than line radiation), and

ii) the central source does not get attenuated (i.e. the medium is *optically thin not only for the continuum radiation, but also for the line itself*), we obtain for the radial line force

$$g_{line}^{thin} = \frac{\pi I_\nu^0 \alpha_L}{\rho c} = \frac{F_\nu^0 \alpha_L}{\rho c} \tag{10}$$

where the latter equality uses $F = \pi I$ for this case of a uniformly bright stellar disc (can you see how this might change if you were to include limb darkening?) and the ^{0} signals that the intensity and flux are taken at the line-centre frequency.

It is now instructive to re-write the optically thin line acceleration as

$$g_{line}^{thin} = \left(\frac{F_\nu^0 \nu_0}{F} \right) \left(\frac{\kappa_e F}{c} \right) \left(\frac{\alpha_L}{\alpha_e \nu_0} \right) = w_\nu g_e q \tag{11}$$

where w_ν weights the line's position in the flux spectrum ($w_\nu \sim 1$ near the peak of the flux-spectrum), g_e is the previously considered force due to electron scattering, and

$$q = \frac{\alpha_L}{\alpha_e \nu_0} = \frac{n}{n_e} f_{lu} \frac{\sigma_{cl}}{\sigma_{Th} \nu_0} = \frac{n}{n_e} f_{lu} \frac{\pi Q}{2} \tag{12}$$

where $Q = 2\pi\nu_0/\gamma$ is the so-called $Q - value$ for the spectral line viewed as a driven, weakly damped, harmonic oscillator with classical damping coefficient γ – that is, it is the *quality* of the resonance; for derivation and some discussions of this, see again Sundqvist's Ch. 4 in radiative processes notes.

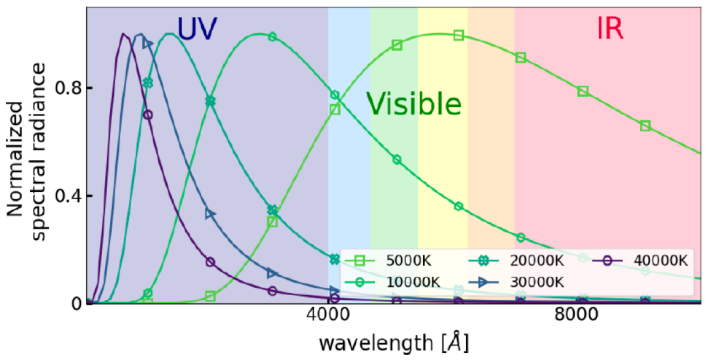

Figure 1.3: The figure demonstrates the normalized spectral radiance versus wavelength (in Å) for different temperatures. The color-marked curves demonstrates the black-body distribution curve for different temperatures. It can be seen that the peak of the black-body curve shifts towards the right-hand side with decreasing temperature, which is governed by Wien's displacement law. In the figure, 'UV' stands for the ultraviolet, 'IR' stands for the infrared, and 'Visible' refers to the visible part of the spectrum. The peak of the black-body distribution curves for the more massive O and B-type stars ($\sim 40000K$ and $\sim 20000K$ respectively) lies in the UV part of the spectrum whereas for sun ($\sim 5000K$) it lies on the visible part of the spectrum.

Figure 1: Figure illustrating the Black-Body spectral distribution for various temperatures. See text. Figure adapted from D. Debnath, KU Leuven Master Thesis (2022).

The key point to realize now is that the "quality" Q of the resonance is extremely large for spectral lines, on order $\sim 10^7$. Assuming an ionized plasma dominated by hydrogen, $n_e \sim n_H$ and for, say, a strong resonance carbon line with abundance $n/n_H \sim 10^{-3...-4}$ and $f_{lu} \sim 1$, we then get $q \sim 10^{3...4}$.

Another important thing to realise from the above expression is that to get some decent amount of line force, we should be relatively close to the object's flux maximum, so that the factor $w_\nu = F_\nu^0 \nu_0 / F$ does not become too small. As an example, for a hot star with $T_{\rm eff} \sim 40kK$, this peak will lie well into the ultraviolet regime, so that lines there are considerably more effective for line-driving than corresponding strong lines in, say, the infra-red; figure 1 illustrates this point for black-body distributions of various temperatures.

Moreover, the above can also demonstrate how the line force will depend on the excitation and ionisation state of the gas, since the number densities n/n_H that enter will be due to specific bound energy levels n_i of various atomic species. Moving a little bit ahead, let me further mention already here that in the end we will be interested in the *total* line force arising from *all* contributing

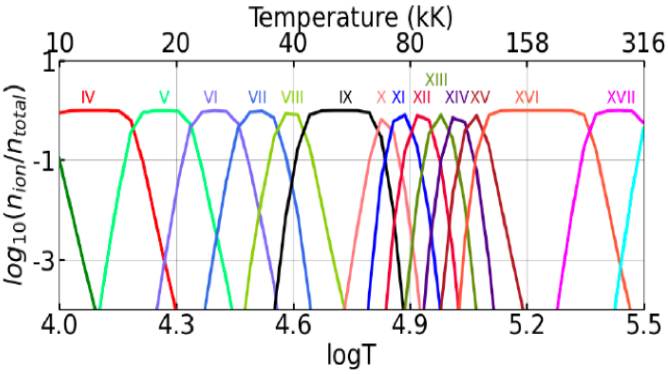

Figure 3.2: Figure illustrating the ionization fraction (n_{ion}/n_{total}) for the ionization stages of iron, for a fixed density of $\rho = 10^{-20}$ $g\ cm^{-3}$. The abscissa displays the logarithmic temperature in Kelvin, and the ordinate represents the normalized ionization fraction. The colors represent the individual ionization stage of iron.

Figure 2: Figure showing ionisation balance of iron assuming LTE. Figure adapted from D. Debnath, KU Leuven Master Thesis (2022).

spectral lines in a given situation, which essentially means that the more lines a certain atomic species can contribute with, the better it will (most often) be to accumulate the total line-force. As a specific example, iron has a lot of lines available. Figure 2 then plots the number density ionisation balance n_{ion} of iron as function of temperature T for a density ρ, computed from the Saha and Boltzmann relations assuming LTE. As we can see from the figure, which lines will be effective line-drivers depend sensitively on the temperature of the radiating gas, where for this (admittedly very low) density e.g. lines from three times ionised iron (Fe IV) will contribute the most at $T \sim 10^{4.1} K$, lines from Fe VI will contribute most significantly at $T \sim 10^{4.4} K$, and so forth.

In summary, the above essentially means that under 'good' conditions the radiative acceleration from only one single optically thin line can exceed that of continuum electron scattering by more than a factor of thousand. Indeed, it is this high quality of the line resonance that makes it possible for the accumulative force from a myriad of spectral lines to overcome gravity and drive supersonic outflows from astrophysical objects such as hot, massive stars, cataclysmic variables, and AGN disks.

However, in reality the above picture becomes more complicated because of the fact that, of course, lines do become optically thick...

2.2 The spectral line force in the Sobolev approximation

The analysis above neglects any attenuation of I_ν. More generally, many lines quite easily become optically thick and I_ν needs to be computed from the radiative transfer equation, whose formal integral is

$$I_\nu(\tau_\nu) = I^0_\nu e^{-\tau_\nu} + \int S(t_\nu) e^{-|\tau_\nu - t_\nu|} dt_\nu = I_{dir} + I_{diff}. \tag{13}$$

To simplify a bit, we will now first make use of some knowledge we already have about the soon-to-be-introduced "Sobolev approximation", applicable in cases with large spatial velocity gradients (e.g. large dv/dr in the case of a radially directed stellar wind). Namely, in such a case the above $I_{diff}(\mu) = I_{diff}(-\mu)$, so that this component vanishes when computing the line force in this Sobolev approximation (for a full derivation of this, you may consult Ch. 6.8 in John Castor's book "radiation-hydrodynamics", available as pdf-book online). We thus write

$$I_\nu(\tau_\nu) = I^0_\nu e^{-\tau_\nu} \tag{14}$$

for *line* optical depth (which can now be arbitrary large, however we continue to neglect attenuation in the *continuum*)

$$\tau_\nu = \int \alpha_L \phi_\nu dl \tag{15}$$

along some direction l. Using the Doppler formula

$$\frac{\nu - \nu_0}{\nu_0} = \frac{v_l}{c} \tag{16}$$

we can transform this from a spatial to a frequency integral

$$\tau_\nu = \int \alpha_L \phi_\nu (dl/d\nu) d\nu = \int \phi_\nu \frac{\alpha_L c}{\nu_0 dv_l/dl} d\nu. \tag{17}$$

Making now the *Sobolev assumption* that the line-of-sight velocity gradient dv_l/dl and the line extinction α_L are approximately constant over the line resonance region, the above can be recast as

$$\tau_\nu = \frac{\alpha_L c}{\nu_0 |dv_l/dl|} \int \phi_\nu d\nu = \tau_S \int \phi_\nu d\nu \tag{18}$$

where the last equality introduces the *Sobolev optical depth*

$$\tau_S = \frac{\alpha_L c}{\nu_0 |dv_l/dl|} = \frac{q \kappa_e \rho c}{|dv_l/dl|} = qt \tag{19}$$

where the last equality casts this in the form of the line-strength parameter q defined above and a characteristic optical-depth variable

$$t \equiv \kappa_e \rho c / |dv_l/dl|. \tag{20}$$

Note i) that since the line profile is normalized, the optical depth integrated over the line becomes equal to this Sobolev optical depth, and ii) τ_S differs from the standard optical depth in being a *local* quantity.

The projected line-of-sight velocity gradient is in general 3D

$$\frac{dv_l}{dl} = \mathbf{n} \cdot \nabla (\mathbf{n} \cdot \mathbf{v}) \tag{21}$$

for spherical symmetry

$$\frac{dv_l}{dl} = \mu^2 \frac{dv_r}{dr} + (1-\mu^2)\frac{v_r}{r} \tag{22}$$

and for the radial streaming approximation $n_r = \cos\theta \equiv \mu = 1$,

$$\frac{dv_l}{dl} = \frac{dv_r}{dr}. \tag{23}$$

Inserting this into our line acceleration expression now gives

$$\mathbf{g}_{line} = \frac{\alpha_L}{\rho c} \oint \int \mathbf{n} I_\nu^0 \phi_\nu e^{-\tau_S \int \phi_\nu d\nu} d\nu \; d\Omega \tag{24}$$

Assuming (for simplicity, it is possible to keep the full vector expression, see again e.g. Castor's Ch. 6.8 in his book "radiation-hydrodynamics") again now spherical symmetry and that I_ν^0 is slowly varying in frequency and non-zero only for a radial direction $\mu = 1$, we can rewrite using $\Phi = \int \phi_\nu d\nu$ and perform the frequency-integral analytically (do this! it's a good exercise, and I will also provide solution for you on toledo page of course..), yielding finally

$$g_{line} = \frac{\alpha_L \pi I_\nu^0}{\rho c}\left(\frac{1-e^{-\tau_S}}{\tau_S}\right) = g_{line}^{thin}\left(\frac{1-e^{-\tau_S}}{\tau_S}\right) \tag{25}$$

where the latter expression uses the expression obtained above for the optically thin case, and where τ_S is understood to now be in the radial direction.

As it should, this key equation recovers the optically thin limit for $\tau_S \ll 1$, but also shows that for an optically thick line with $\tau_S \gg 1$, the thin line force is reduced by

$$g_{line}^{thick} = \frac{g_{line}^{thin}}{\tau_S} = w_\nu \frac{F}{c^2}\frac{dv_r/dr}{\rho}. \tag{26}$$

This now shows that the radiation force per unit mass is *independent* of the atomic opacity, and instead proportional to the spatial velocity gradient in the flow; a neat discussion on the physics of this quite remarkable property can be found in Castor's book (toward end of his Ch. 6.8).

Note that the above analysis never needs to specify explicitly how the line profile behaves within the line resonance zone. In order to evaluate the validity of the Sobolev approximation, however, one needs to do so. For example, for a Doppler profile of characteristic width $v_{th} = \sqrt{2kT/m}$, the opacity in a radial streaming model needs to be roughly constant over a few radial *Sobolev lengths* $\Delta r \approx v_{th}/(dv/dr) = L_{Sob}$. As illustrated in Figure 3 below, if this condition is valid then the hydrodynamical conditions will be roughly constant over the complete *line resonance zone*, defined by the region in which the frequencies 'seen' by the moving gas particles (the co-moving frequency) have been Doppler shifted into resonance with the spectral line of interest.

Exercise: Compute the radial Sobolev length L_{Sob} in the wind of a massive star with $v_{th} \approx 10$ km/s and typical velocity gradient $dv/dr \approx v/r$ for $v \approx 1000$ km/s and $r \approx R_*$. Express your answers in units of the stellar radius R_*.

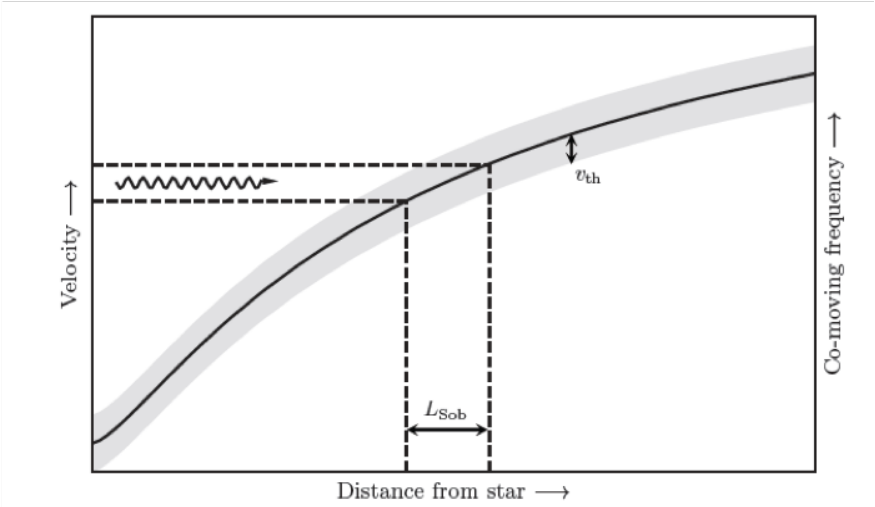

Figure 2.1. Cartoon of a monotonically increasing wind velocity profile (black solid line). The line-resonance zone is set by the thermal speed $v_{\rm th}$ of an exemplar line profile (grey area). Photons emitted at the star (left) travel until they have the correct co-moving frequency to go into resonance and scatter through a few Sobolev lengths $L_{\rm S}$ within the line.

Figure 3: Figure illustrating the Sobolev approximation, with $L_S = L_{Sob}$ in these lecture notes. See text. Figure adapted from Florian Driessen, KU Leuven PhD Thesis (2022).

2.3 Extra Side-Note: Wind "performance" and mass loss from a single optically thick line

To gain further physical insight about the radiation force $g_{\rm rad} = \kappa_F F/c$, here now written for some generic flux-weighted opacity κ_F, let's assume it works on a spherical shell of mass $dm = 4\pi r^2 \rho dr$, so that NII gives

$$\text{ma} = \text{force} \rightarrow dm\, a = dm\, v\frac{dv}{dr} = dm\, \frac{\kappa_F F}{c} \tag{27}$$

for steady-state acceleration $a = dv/dt = \partial v/\partial t + v dv/dr = v dv/dr$. Using mass-conservation $\dot{M} = 4\pi r^2 \rho v$ and $L = F 4\pi r^2$, this gives

$$\dot{M} dv = \frac{L}{c}\rho\kappa_F dr = \frac{L}{c} d\tau, \tag{28}$$

which integrated over the wind until terminal velocity $v(r \rightarrow \infty) = v_\infty$ is

$$\dot{M} v_\infty = \frac{L}{c}\tau \tag{29}$$

for total wind optical depth $\tau = \int \rho\kappa_F dr$, which is here equal to the ratio of wind to radiative momentum

$$\eta = \dot{M} v_\infty c/L = \tau, \tag{30}$$

showing how this so-called "wind performance number" η is linked to the total flux-weighted optical depth of the wind.

The above applies quite generally for a radiative force. Using now *specifically* the optically thick line force from above to balance inertia in the e.o.m. gives

$$v\frac{dv}{dr} = w_\nu \frac{F}{c^2}\frac{dv_r/dr}{\rho} \tag{31}$$

giving directly an estimate for the maximum mass-loss rate that can be driven by such a single optically thick line

$$\dot{M} = w_\nu \frac{L}{c^2} \tag{32}$$

Exercise: Assume now that the radiation force must balance the *sum* of inertia and gravitational acceleration. How will results for η and $\dot{M}$ for a single optically thick line above change?

3 CAK-like model for wind driven by an ensemble of spectral lines

Using the above results, it is often useful to normalise the line-force from a single line to that stemming from electron scattering

$$\frac{g_{line}}{g_e} = w_\nu q \left(\frac{1 - e^{-qt}}{qt} \right) \tag{33}$$

3.1 Summation over all contributing lines

To evaluate the line-force stemming from a large ensemble of spectral lines, we sum over all contributing lines i,

$$\frac{g_{line}^{tot}}{g_e} \equiv M(t) = \sum_i w_{\nu,i} q_i \left(\frac{1 - e^{-q_i t}}{q_i t} \right), \tag{34}$$

where $M(t)$ is the so-called *line-force multiplier*. Note that this effectively assumes that lines do not intrinsically overlap in frequency-space, i.e., all lines can be taken as separate integrals and so contribute fully to the total frequency-integrated radiation force.[1]

The question then becomes how to practically evaluate this sum, especially since in a given situation many, many thousand of lines can be contributing to the total line-force.

In the case that all lines become optically thin, $tq_i \ll 1$, we obtain directly

$$M(tq_i \ll 1) = \sum_i w_{\nu,i} q_i \equiv \bar{Q} \tag{35}$$

where the latter defines the parameter $\bar{Q}$ (Gayley 2000) as the line-force enhancement factor as compared to the Thomson scattering force in the case all lines are optically thin. In a real physical situation, however, we will have a mix of optically thin and thick lines to account for.

3.2 CAK-like theory for accumulative line-force from an ensemble of lines

The groundbreaking Castor-Abbott-Klein (1975) paper (CAK) computed the sum above based on a set of doubly ionised carbon atomic data and by assuming local thermodynamic equilibrium (LTE) for the carbon atoms and a Plankian illuminating radiation field. They then observed that, in a range relevant for steady winds from O-supergiants, the computed line-force sum behaved like an inverse power-law $M(t) \propto 1/t^\alpha$, and proceeded to provide line-force fits on the form $M(t) = k/t^\alpha$, where k is a constant.

Moreover, they then also showed that such a line-force behaviour calculated from the full summation may be understood by assuming that the sum be replaced by a distribution function over the number of lines with certain line-strength. That is,

$$M(t) = \sum_i w_{\nu,i} q_i \left(\frac{1 - e^{-q_i t}}{q_i t} \right) \approx \int \left(\frac{g_{line}}{g_e} \right) \frac{dN}{dq} dq, \tag{36}$$

[1] We note that this assumption indeed sometimes can be an issue, for example in very dense winds and in spectral windows where we might have very many contributing lines of similar rest-frequencies.

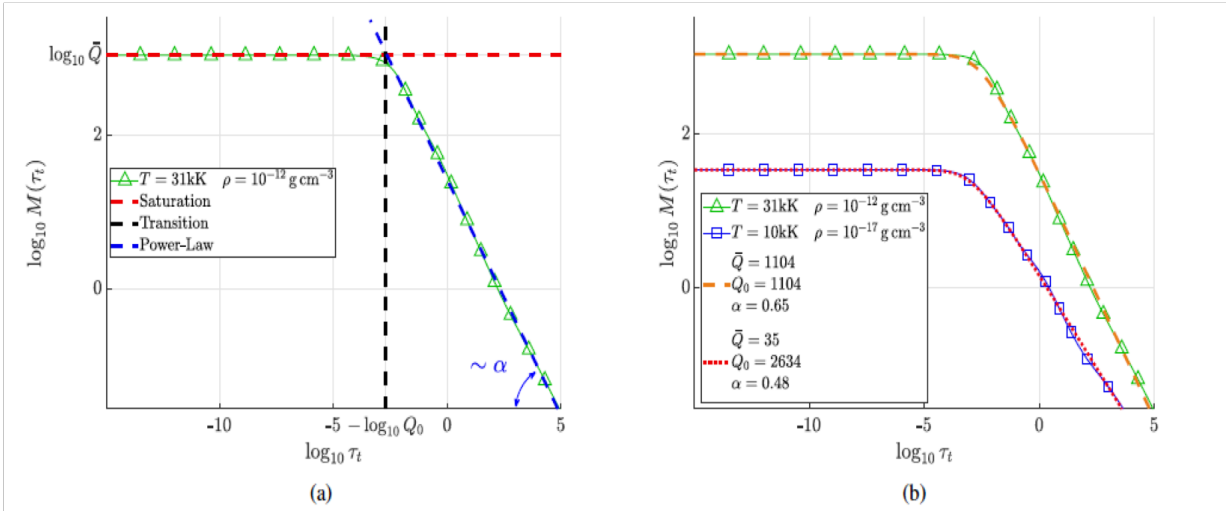

Fig. 1: Force multiplier as computed by evaluating the numerical sum over the discrete set of spectral lines in the triangle-marked green curve. Panel (a) shows the saturation level indicated in a red-dashed curve, a power-law region in the blue-dashed line, and the location of a transition point in the black-dashed line. Panel (b) shows the actual fit of two numerical results, where triangle-marked green line has the same temperature and density as in (a) and the square-marked blue line assumes a different set of temperature and density. The derived fit parameters for each case are indicated in the corresponding legend.

Figure 4: Figure illustrating fits of the line-force to an analytic function. In figure, the parameter $\tau_t = t$ in these lecture-notes. See text. Figure adapted from Poniatowski et al. (2022).

where in the original CAK-model the flux-weighted line-strength distribution function was assumed to follow a simple power-law of index $\alpha-2$, $dN \propto q^{\alpha-2}dq$. More modern approaches typically truncate the power-law distribution using an exponential cut-off at the high end (physically motivated because lines cannot be infinitely strong). In Poniatowski et al. (2022), a flux-weighted distribution-function

$$\frac{dN}{dq} = \frac{\bar{Q}}{\Gamma(q)Q_0^2}\left(\frac{q}{\bar{Q}_0}\right)^{\alpha-2} e^{-q/Q_0} \tag{37}$$

is assumed, where $\Gamma(\alpha)$ now represents the Gamma function (NOT to be confused with Eddington's gamma representing the ratio of radiation to gravitational acceleration!) and the line-strength normalization constant $\bar{Q}$ and cut-off Q_0 used are due to Gayley (1995). Using this distribution and assuming a frequency distribution $\sim \nu^{-1}$, the total line force is evaluated analytically to yield for the force-multiplier

$$M_{fit}(t) = \frac{\bar{Q}}{(1-\alpha)}\frac{(1+Q_0 t)^{1-\alpha}-1}{Q_0 t}. \tag{38}$$

The physical interpretation of $\bar{Q}$ as the line-force enhancement factor as compared to the Thomson scattering force in the case all lines are optically thin ($\alpha = 0$) becomes clear from this expression. Due to the blending of optically thin and thick lines, however, this maximum enhancement is reduced by a typical factor $(Q_0 t)^{\alpha}$, with α representing the ratio of the line force contribution from

optically thin lines to the total line force.

The expression above lends itself well to tabulations of the force-multiplier, in the same spirit as tabulations of for example Rosseland mean opacities in a static medium (e.g., the 'OPAL' opacity tables). Fig. 1 shows prototypical examples where the complete sum eqn. 34 is fitted by eqn. 38 as function of t for given pairs of (ρ, T); the ionisation and excitation balance (to get all q_i) are here computed for the given ρ and T from the Saha-Boltzmann relations (LTE) and an illuminating black-body radiation field (to get w_i). The atomic data come from the 'Munich line data-base', consisting of some $4-5$ millions spectral lines in relevant ionisation stages, compiled first by Adi Pauldrach and Jo Puls; see Poniatowski et al. (2022) for more details. This figure demonstrates directly some important qualitative features of the line-force:

i) a saturation level in the optically thin limit is indeed found, consistent with definition of $\bar{Q}$,
ii) the turn-over is directly related to parameter Q_0,
iii) α represents the overall steepness of the line-strength distribution once lines start becoming optically thick.

Let me point out here that different normalisations for the CAK line-force occur in the literature. For example, the original CAK paper did not include the saturation in the optically thin limit and used a different parameter (k above) for their normalisation. The two different parametrisations are equivalent if one makers the ansatz $\bar{Q} = Q_0$ in the above and then consider only the limit $\bar{Q}t \gg 1$; however, it is important to keep in mind that this may not always be a very good assumption. The book by Lamers & Cassenelli also uses another formulation than here, which also does not account for some of the effects discussed above. Papers by Ken Gayley (1995), Jo Puls et al. (2000), and Luka Poniatowski et al. (2022) make comparisons and discuss these subtle differences further. Overall though, regardless of parametrisation a resulting key property is: $g_{line}^{CAK} \propto Lr^{-2}(dv/dr/\rho)^{\alpha}$.

Incorporation of this radiation force (or extensions of it) into the radiation-hydrodynamics equations now provides a good rationale for computations of supersonic wind outflows from hot, luminous stars that are much more massive than our Sun.

Moreover, based on the above line force and a simplified equation-of-motion we can derive very insightful and useful expressions and scaling relations for the global wind parameters $\dot{M}$ and v_∞.

3.3 Analytic CAK velocity law and mass loss for line-driven wind

To derive analytic scaling relations for mass-loss rate and velocity law, we first make the simplifications discussed above by assuming $\bar{Q} = Q_0$ and consider the 'power-law' limit $\bar{Q}t \gg 1$. Then eqn. 38 simplifies to the original CAK-expression

$$M_{CAK}(t) = \frac{g_{line}^{CAK}}{g_e} = \frac{\bar{Q}}{(1-\alpha)} \frac{1}{(\bar{Q}t)^{\alpha}}. \tag{39}$$

Let us then again consider the supersonic limit $v \gg a$. Dropping then the 'Parker term" (see previous discussion) the equation of motion for a steady, spherical stellar wind driven by the line force (+ continuum Thomson scattering) is

$$v\frac{dv}{dr} = g_{line}^{CAK} + g_e - g. \tag{40}$$

Introducing the variable

$$w' \equiv \frac{r^2 v dv/dr}{GM(1-\Gamma_e)} = \frac{dw}{dx} \tag{41}$$

for

$$w \equiv \frac{v^2}{v_{esc,eff}^2} = \frac{v^2}{2GM(1-\Gamma_e)/R_*} \tag{42}$$

with the "effective" (reduced by Thomson scattering $\Gamma_e < 1$) escape speed $v_{esc,eff}$ from the stellar surface R_*, and

$$x \equiv 1 - R_*/r \tag{43}$$

Exercise: Show that the CAK equation of motion above can be written as

$$w' = C(w')^\alpha - 1 \tag{44}$$

for constant

$$C = \frac{1}{1-\alpha}\left(\frac{\bar{Q}\Gamma_e}{1-\Gamma_e}\right)^{1-\alpha}\left(\frac{L}{\dot{M}c^2}\right)^\alpha. \tag{45}$$

Depending on the value of the constant C, eq. 44 can have zero, one, or two solutions, where the CAK model represents the critical value for which only one solution is found:

$$F(w') = w' + 1 - C_c(w')^\alpha = 0 \tag{46}$$

$$\frac{\partial F}{\partial w'} = 1 - \alpha C_c (w')^{\alpha-1} = 0. \tag{47}$$

This gives us two equations for the two unknowns C_c and w', and so we can readily solve it to yield

$$C_c = \frac{1}{\alpha^\alpha (1-\alpha)^{1-\alpha}} \tag{48}$$

and

$$w'_c = \frac{\alpha}{1-\alpha} \tag{49}$$

giving directly the CAK mass-loss rate and velocity law

$$\dot{M}_{CAK} = \frac{L}{c^2}\frac{\alpha}{1-\alpha}\left(\frac{\bar{Q}\Gamma_e}{1-\Gamma_e}\right)^{1/\alpha-1} \tag{50}$$

$$v(r) = v_\infty \left(1 - \frac{R_*}{r}\right)^\beta \tag{51}$$

Exercise: For this CAK model, show that $\beta = 1/2$ and $v_\infty = v_{esc,eff}\sqrt{\alpha/(1-\alpha)}$.

Inserting typical values for a luminous O-star, $L \approx 8 \times 10^5 L_\odot$, $\Gamma_e \approx 0.4$, and $v_{esc,eff} \approx 800$ km/s, we find $\dot{M} \approx 4.0 \times 10^{-6}\,\mathrm{M}_\odot$/yr and $v_\infty \approx 1100$ km/s for $\bar{Q} \approx 2000$ and $\alpha \approx 2/3$.

The values obtained from this simple theory are actually in reasonable agreement with empirically obtained values (derived e.g. from fitting synthetic spectra to observations), but can be significantly improved by, e.g., dropping the radial streaming approximation and accounting also for the finite extent of the stellar disc (see below). Note that both mass-loss rates and wind speeds are high; line-driven winds are typically both very strong and very fast.

In comparison to the the dust-driven winds from cool, evolved stars, the mass-loss rates are quite similar but the wind speeds drastically different (such dust-driven winds are much slower); using the very simple "$\sim r^{-2}$" model outlined first in these notes, you can readily verify that this to some extent can be understood simply by the vastly different escape speeds of the relatively compact hot stars and the very extended cool stars.

3.4 Extensions of the basic CAK model

3.4.1 Finite-disc correction factor

As mentioned, the above analysis assumes radially streaming photons from a stellar photosphere into the surrounding wind. But though this is a good approximation at large distances from that photosphere, close to the star non-radial photons may play an important role; the situation is sketched in Fig. 5.

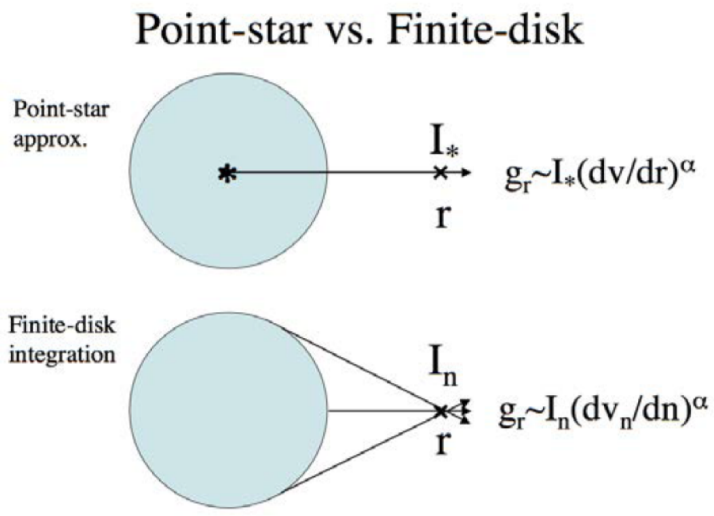

Figure 5: Figure illustrating the so-called finite-disc factor. Sketch with courtesy of Stan Owocki.

To evaluate this factor, let's go back to our general expression in the first section for the radiation force from a single line,

$$\mathbf{g}_{line} = \frac{\alpha_L}{\rho c} \oint \int \mathbf{n} I_\nu^0 \phi_\nu e^{-\tau_S \int \phi_\nu d\nu} d\nu \; d\Omega. \tag{52}$$

The key point is that although the frequency integration still can be carried out as before, we must now keep the angle integral unevaluated. Using the distribution-function for an ensemble of lines as discussed above, we obtain

$$M_{fd}(t) = \frac{\bar{Q}}{1-\alpha} \oint I_* \mathbf{n} \frac{(1+Q_0 t(\mathbf{n}))^{1-\alpha} - 1}{Q_0 t(\mathbf{n})} \; d\Omega. \tag{53}$$

This expression now gives the radial component of the line-force if $\mathbf{n} = \cos\theta = \mu$; in a general 3D situation, also the other two line-force vector-components can be non-zero and the integral has to be evaluated numerically. However, for a 1D, radial and stationary wind with core intensity I_* constant across the star (neglecting e.g. limb-darkening), we may solve the integral analytically to obtain (CAK, Friend & Abbott 1986; Pauldrach et al. 1986):

$$f_d = \frac{(1+\sigma)^{1+\alpha} - (1+\sigma\mu_*^2)^{1+\alpha}}{(1+\alpha)(1-\mu_*^2)(1+\sigma)^\alpha \sigma} \tag{54}$$

for

$$f_d \equiv \frac{M_{fd}}{M_{rs}} \tag{55}$$

the finite-disc correction-factor as compared to the line-force (or force-multiplier) M_{rs} evaluated in the radial streaming approximation. Here $\sigma \equiv d\ln v / d\ln r - 1$ and $\mu_*^2 \equiv 1 - R_{core}^2/r^2$ for stellar core radius R_{core}. We note how the *radial* component of the lien-force now also depends on the *non-radial* velocity gradient components.

Exercise: Derive and verify the above expression for the 1D finite-disc correction factor f_d.

For the 1D, steady O-star case, comparison to the radial streaming approximation typically shows that the finite-disc corrected line-force becomes somewhat lower in regions close to the photosphere ($f_d < 1$), while still (of course) eventually reaching the radial streaming value at large distances ($f_d = 1$, as it should per definition). This has the effect of moving the spatial place where it is 'hardest' to sustain the wind-outflow against gravity to very close to the core radius, so that the steady-state mass-loss rate effectively is determined in those layers close to the star. Since at the lower wind boundary $r \to R_{core}$ (often assumed to precisely coincide with the optical stellar surface, i.e. $R_{core} = R_*$) we have $\mu_* \to 1$, $v \to 0$, $\sigma \to \infty$, one obtains $f_d(r \to R_{core}) \equiv f_d^* = 1/(1+\alpha)$.

If we then assume the mass-loss rate is set at this point (effectively we're assuming that the so-called wind critical point lies here), one can then also derive a finite-disc correction factor to the analytic expression for mass-loss rate in the CAK model

$$\dot{M}_{fd} = (f_d^*)^{1/\alpha} \dot{M}_{CAK}. \tag{56}$$

For a typical $\alpha \approx 2/3$, this thus has the effect of lowering the mass-loss rate by a factor of ~ 2. Moreover, since the mass-loss rate now has been lowered and the finite-disc factor increases from its minimum value as we move away from R_*, the lower mass-loss rate now means the wind can be accelerated to higher velocities. Since the line-force now has a quite intricate radial dependence, the equation of motion has to be solved numerically, with the general results that for steady O-star winds we get a somewhat 'smoother' $\beta > 0.5$) overall acceleration profile and a significantly (factor of two or more) higher terminal wind speed v_∞ as compared to the radial streaming model (see Owocki 2003 for further discussion and illustrations). Observationally, these general trends overall agree well with various empirical studies of populations of O-star winds aiming to derive global wind parameters.

3.4.2 Semi-analytic 'cooking recipe' for line-driven mass-loss rates including finite-disk, sound speed, and $Q_0 \neq \bar{Q}$

If $Q_0 \neq \bar{Q}$, the above equation 39 for the mass-loss rate has to be corrected for by an extra factor $Q_0/\bar{Q}$ (see Gayley 1995). The finite-disk corrected final mass-loss rate formula is thus:

$$\dot{M}_{CAK} \approx \frac{L}{c^2}\frac{\alpha}{1-\alpha}\left(\frac{\bar{Q}\Gamma_e}{1-\Gamma_e}\right)^{1/\alpha-1}\frac{Q_0}{\bar{Q}}\left(\frac{1}{1+\alpha}\right)^{1/\alpha} \tag{57}$$

Now re-inserting our typical values for a luminous O-star in the Milky Way, $L \approx 8\times10^5 L_\odot$, $\Gamma_e \approx 0.4$, and $v_{esc,eff} \approx 800$ km/s, we find $\dot{M} \approx 2.0 \times 10^{-6}\,\mathrm{M}_\odot$/yr and $v_\infty \approx 2200$ km/s for $\bar{Q} \approx Q_0 \approx 2000$ and $\alpha \approx 2/3$.

It is also possible to include an analytic correction factor to the small, but finite, gas sound speed (see Appendix in Owocki & ud-Doula 2004). To derive $\dot{M}$ for such a modified finite disk and sound speed corrected model then, the problem is thus reduced to find what the line-force parameters are at the wind critical point that sets the now slightly modified CAK-like line-driven mass-loss rate; that is, we need $\bar{Q}^{cr}$, Q_0^{cr}, α^{cr}. For this we can use the tabulations from Poniatowski et al. (2022) and Debnath et al. (2022) discussed above and devise a very simple algorithm:

- Make a first guess for $\bar{Q}^{cr}$, Q_0^{cr}, α^{cr}.
- Compute $\dot{M}$ analytically according to the above.
- From this, update density at critical point via $\rho_{cr} = \dot{M}/(4\pi r_{cr}^2 v_{cr})$.
- Use the updated density to compute new $\bar{Q}^{cr}$, Q_0^{cr}, α^{cr}.

Since the wind critical point when including the finite-disk correction factor is close to the stellar surface (see above), we can approximate $r_{cr} \approx R_\star$ and furthermore $T \approx T_{eff}$ in the above. To find the wind critical velocity we further use equation 55a from the classical 'cooking recipe' by Kudritzki et al. (1989). With these assumptions the only parameter left to find is the wind density at the critical point ρ_{cr}, and the above simple algorithm typically converges within a few iterations.

This now allows us to easily explore how line-driven mass-loss rates behave as functions of the stellar parameters. Fig. 6 plots mass-loss rates computed in this way for stars with different effective temperature T_{eff} and luminosities L but the same mass $40M_\odot$ and a metallicity equal to that of the Sun; the oordinates show the (electron scattering) Γ_e and the abscissae the stellar

effective temperatures. From the top left panel of this plot, we can directly see how mass-loss rates are highest in the top right corner (highest L/M ratio and T_{eff}) and lowest in the bottom left (lowest L/M and lowest T_{eff}). The bottom panels of this figure further plot the values of the line-force parameters at the wind critical point. Interestingly, there is a small decrease in α_{cr} for lower T_{eff}, indicating relatively more contributions from optically thin lines. Such a decrease in α could actually have led to a corresponding increase in mass-loss rate (see above relations), but we note how this potential effect in practise is counteracted by low ratios of $Q_0/\bar{Q}$ in this regime and also by a drop in the absolute values of $\bar{Q}$. Finally, for completion the middle and right top panels of the figure compare these (semi-)analytic rates to the ones computed by the different methods by Bjorklund et al. (2023) (here at KU Leuven) and Vink et al. (2001), as these two alternative mass-loss 'recipes' are popular to include in various applications like stellar evolution.

Fig. 7 then takes out three values of Γ_e from the above models and display the values of the critical line-force parameters in a temperature-density diagram. From these, we can directly inspect how α, Q_0, and $\bar{Q}$ behave as functions of these parameters. In particular, we may note that while indeed there is quite a strong tendency to find lower value for α for lower temperatures, when evaluating mass-loss rates this effect is also somewhat moderated by a simultaneous decrease in critical-point density for models with lower temperatures but the same Γ_e and mass. Finally, although not shown explicitly here similar maps can be used to explore more aspects of line-driving, such as the dependence on stellar metallicity

essentially, $\bar{Q} \sim Z$, which to first order gives $\dot{M} \sim Z^{1/\alpha-1}$.

3.4.3 Further extensions

Not yet. Examples of topics that could be covered: 3D line force for rotating stars or stars still in formation process; radiation line-driven instability ('LDI'); interaction with a magnetic field, radiation-driven winds that are optically thick in the continuum (WRs, LBVs, etc).

4 References

Castor, J. I. 2004, Radiation Hydrodynamics

Castor, J. I., Abbott, D. C., & Klein, R. I. 1975, ApJ, 195, 157

Debnath, D., Master Thesis, 'Updating Atomic Data Base for Astrophysical Applications: first results for WR-stars'

Driessen, F.A., (2022), PhD Thesis, 'The line-deshadowing instability and its effects on wind clumping for OB-stars'

Friend, D. B. & Abbott, D. C. 1986, ApJ, 311, 701

Gayley, K. G. 1995, ApJ, 454, 410

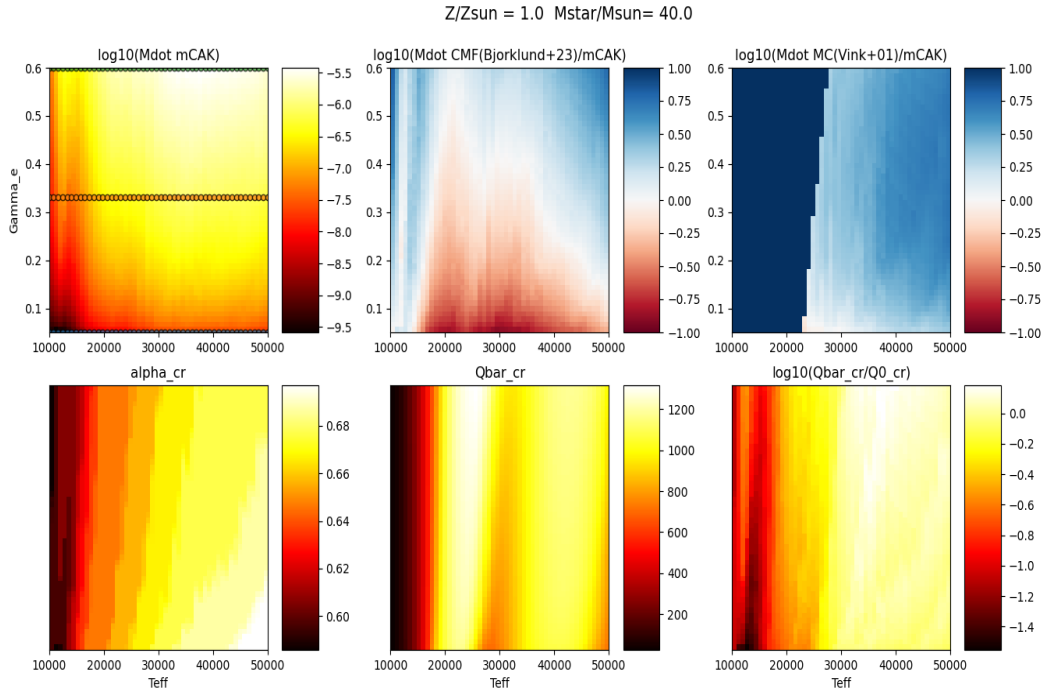

Figure 6: Mass-loss rates (in units of solar masses per year, $M_{\odot}/yr$) and critical values of the line force parameters α, $\bar{Q}$, and Q_0, for stars with a range of effective temperatures and luminosities, but fixed mass and metallicity. Y-axis displays $\Gamma_e \propto L/M$ and x-axis T_{eff}.

Lamers & Cassinelli (1999), Introduction to stellar winds

Owocki, S.P. 2004, 'Stellar wind mechanisms and instabilities'

Pauldrach, A., Puls, J., & Kudritzki, R. P. 1986, A&A, 164, 86

Poniatowski, L.M., et al. 2022, A&A, 667A

Puls, J., Springmann, U., & Lennon, M. 2000, A&AS, 141, 23

Sundqvist, Jon, Lecture notes 'radiative processes in astronomy'

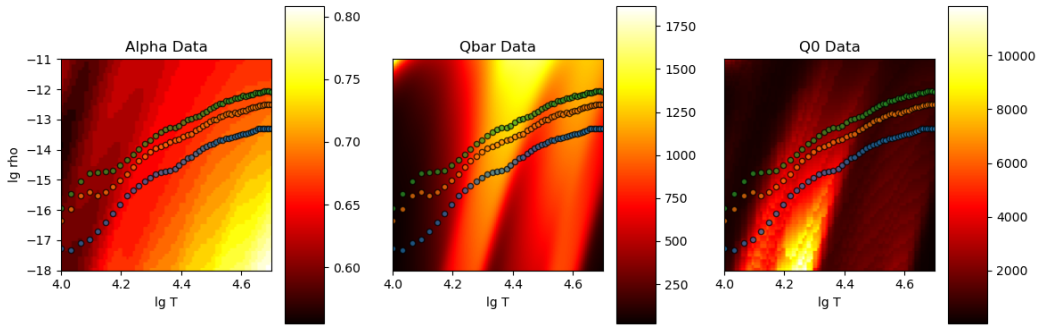

Figure 7: α, $\bar{Q}$, and Q_0 as functions of temperature T and density ρ. The three curves in the figures denote the stars as indicated by the same curves in the previous figure.